Chapter 8
Cylindrical Wave Method for Pure and Doped Nanotubes

P.N. D'Yachkov

Abstract The study results on the electronic structure of single-walled and double-walled nanotubes, both pure and doped, isolated and embedded into a crystal matrix and calculated using a linear augmented cylindrical wave method are presented. The method utilizes the local density functional approximation and the muffin-tin approximation for the electron potential and is implemented as a quantum-mechanical program package.

Keywords Nanotubes • Electronic structure • Cylindrical waves

8.1 Introduction

Carbon nanotubes are an important class of nanomaterials. Understanding the electronic properties of nanotubes is important for several current and developing materials-science applications. Theoretical studies of the nanotubes electronic structure have received much attention since 1992, when the first calculations for the band structures of single-wall nanotubes (SWNTs) were carried out using the linear combination of atomic orbitals (LCAOs) π-electronic technique. We develop a new quantum-mechanical method for calculating the electronic structure of single-wall, double-wall, and embedded nanotubes both perfect and having impurities. This is the linear augmented cylindrical wave (LACW) method. The LACW technique, as applied to nanotubes, has an advantage over the conventional

P.N. D'Yachkov (✉)
Institute of General and Inorganic Chemistry, Russian Academy of Sciences,
Leninskii pr. 31, Moscow 119991, Russia
e-mail: p_dyachkov@rambler.ru

Y.N. Shunin and A.E. Kiv (eds.), *Nanodevices and Nanomaterials for Ecological Security*, NATO Science for Peace and Security Series B: Physics and Biophysics, DOI 10.1007/978-94-007-4119-5_8,
© Springer Science+Business Media Dordrecht 2012

LCAO and plane-wave pseudopotential methods. The main argument for using cylindrical waves is to account for the cylindrical geometry of the nanotubes in an explicit form that offers obvious advantages.

8.2 Single-Walled Armchair and Zig-Zag Nanotubes

In the LACW method, a one-electron model is used, implying that a many-electron wave function is described by the determinant of one-electron functions. Then, the problem of calculation of electron levels is reduced to solution of the one-electron Schrödinger equation, where Hamiltonian includes the operators of the kinetic and potential energy of electrons. In calculations of a many-electron system, the key problem is the choice of electron potential. In the LACW method, this potential is constructed with the use of the muffin-tin (MT) approximation and the local density functional approximation for exchange interaction. The MT approximation implies that the crystal space is divided into regions of two types: atomic regions and interatomic regions. Each atom of a polyatomic system is surrounded by a sphere (MT sphere). In the MT spheres, the potential is taken as spherically symmetric. In the interatomic region, the electron potential is taken to be constant. This potential is chosen as the energy reference. The radii of MT spheres are selected so that the spheres of neighboring atoms are in contact. Such a choice is physically rather evident: information on the chemical nature of atoms constituting a polyatomic system is contained only inside the MT spheres. In a nanomaterial, the movement of electrons is restricted by its dimensions and geometry. In a nanotube, electron motion is confined to an approximately cylindrical layer with a thickness on the order of the doubled van der Waals radius of the atom. Correspondingly, in the LACW method, the motion of electrons in the space between MT spheres is limited by two cylindrical barriers impenetrable for electrons: the external barrier Ω_a of radius $\boldsymbol{a}$ and the internal barrier Ω_b of radius $\boldsymbol{b}$ which are chosen so that the region confined by these barriers accommodates a significant portion of the electron density of the system under consideration. Such a potential is referred to as a cylindrical MT potential.

To calculate the potential in the MT spheres, the electron density distribution $\rho(\mathbf{r})$ of a system is constructed as a superposition of electron densities of its atoms. Inside the MT spheres, its spherically symmetric part $\rho(r)$ is taken. The electrostatic potential created by the distribution $\rho(r)$ is determined from the solution of the Poisson equation. The Coulomb potential in the MT spheres is obtained by adding the electrostatic potential created by the positive charges of atomic nuclei. The electron density distribution $\rho(r)$ is also used for calculations of the exchange interaction in the local density functional approximation.

In the interspherical region, the basis functions are the solutions of the Schrödinger equation for free movement of electrons inside an infinite tube with outer and inner radii a and b, respectively. When expressed in rydbergs

(Planck constant $\hbar = 1$, electron mass $m = 1/2$, electron charge $e = \sqrt{2}$) and cylindrical coordinates {Z,Φ,R}, this equation takes the form [1–5]:

$$\left\{-\left[\frac{1}{R}\frac{\partial}{\partial R}\left(R\frac{\partial}{\partial R}\right)+\frac{1}{R^2}\frac{\partial^2}{\partial\Phi^2}+\frac{\partial^2}{\partial Z^2}\right]+U(R)\right\}\times \\ \times\Psi(Z,\Phi,R)=E\Psi(Z,\Phi,R) \tag{8.1}$$

The potential $U(R)$, determining the region in which electrons of an isolated nanotube are allowed to move, takes the form

$$U(R)=\begin{cases}0, & b\le R\le a\\ \infty, & R<b, R>a\end{cases}. \tag{8.2}$$

The solution of Eq. 8.1, taking into account Eq. 8.2, has the form $\Psi(Z,\Phi,R)=\Psi_P(Z)\Psi_M(\Phi)\Psi_{MN}(R)$. Here,

$$\Psi_P(Z)=\frac{1}{\sqrt{c}}exp[i(k+k_P)Z], k_P=(2\pi/c)P, \quad P=0,\pm1,\pm2,\ldots \tag{8.3}$$

is the wave function that describes the free movement of an electron along the translational symmetry axis Z with the period c. The wave vector k belongs to the one-dimensional Brillouin zone: $-\pi/c\le k\le\pi/c$. The function

$$\Psi_M(\Phi)=\frac{1}{\sqrt{2\pi}}e^{iM\Phi}, \quad M=0,\pm1,\pm2,\ldots \tag{8.4}$$

describes the rotation of the electron about the symmetry axis of the system, and the function $\Psi_{MN}(R)$, determining the radial movement of the electron, is the solution of the equation

$$\left[-\frac{1}{R}\frac{d}{dR}R\frac{d}{dR}+\frac{M^2}{R^2}\right]\Psi_{MN}(R)+ \\ +U(R)\Psi_{MN}(R)=E_{|M|,N}\Psi_{MN}(R). \tag{8.5}$$

Here, N is the radial quantum number and $E_{|M|,N}$ is the energy spectrum; the energy

$$E=(k+k_P)^2+E_{|M|,N}, \tag{8.6}$$

corresponds to the wave function Ψ (Z, Φ, R). At $b\le R\le a$, Eq. 8.6 is written as

$$\left[\frac{d^2}{dR^2}+\frac{1}{R}\frac{d}{dR}+\kappa^2_{|M|,N}-\frac{M^2}{R^2}\right]\Psi_{MN}(R)=0, \tag{8.7}$$

where $\kappa_{|M|,N} = \left\{E_{|M|,N}\right\}^{1/2}$. After substituting $\kappa R = \mathrm{x}$ and $\Psi(R) = y(x)$ into Eq. 8.7, it reduces to the Bessel equation. Its solutions are referred to as cylindrical functions of the Mth order. Any solution of the Bessel equation can be represented as a linear combination of cylindrical Bessel functions of the first J_M and second Y_M kinds:

$$\Psi_{MN}(R) = C^J_{MN} J_M\left(\kappa_{|M|,N} R\right) + C^Y_{MN} Y_M\left(\kappa_{|M|,N} R\right). \tag{8.8}$$

In Eq. 8.10, C^J_{MN} and $C^Y_{MN}$are constants chosen so as to ensure the normalization of the wave function $\Psi_{MN}(R)$,

$$\int_b^a |\Psi_{MN}(R)|^2 R dR = 1, \tag{8.9}$$

and its vanishing at the interior and exterior potential barriers. Thus, the basis function Ψ (k, P, M, N) in the Ω_{II} region in the general cylindrical coordinate system takes the form

$$\begin{aligned}\Psi_{II}(k,P,M,N) &= \frac{1}{\sqrt{2\pi c}} \exp\{i(K_P Z + M\Phi)\}\times \\ &\times \left[C^J_{MN} J_M\left(\kappa_{|M|,N} R\right) + C^Y_{MN} Y_M\left(\kappa_{|M|,N} R\right)\right]\end{aligned} \tag{8.10}$$

Here, $K_P = k + k_P$.

Inside the MT sphere α in the local spherical coordinate system {r, θ, φ}, the basis function is expanded in spherical harmonics $Y_{lm}(\theta, \varphi)$ [1, 2]:

$$\begin{aligned}&\Psi_{I\alpha}(r,\theta,\varphi|k,P,M,N) = \\ &\sum_{l=0}^{\infty} \sum_{m=-l}^{l} \left[A_{lm\alpha} u_{l\alpha}(r, E_{l\alpha}) + B_{lm\alpha}\, \dot{u}_{l\alpha}\,(r, E_{l\alpha})\right] Y_{lm}(\theta,\varphi).\end{aligned} \tag{8.11}$$

In Eq. 8.20, $u_{l\alpha}$ is the solution of the radial Schrödinger equation in the MT sphere α for the energy$E_{l\alpha}$, and $\dot{u}_{l\alpha} = [\partial u_{l\alpha}/\partial E]_{E_{l\alpha}}$

$$H_{MT\alpha} u_{l\alpha}(r) = E_{l\alpha} u_{l\alpha}(r). \tag{8.12}$$

Inside the MT sphere of radius r_α, the $u_{l\alpha}$ function is taken to be normalized and the $u_{l\alpha}(r)$ and $\dot{u}_{l\alpha}(r)$ functions are orthogonal.

The desired solutions of the Schrödinger equation must be everywhere continuous and differentiable; therefore, to construct basis functions, the solutions of the wave equation for the interspherical region and MT spheres should be sewn

together. This can be achieved by selecting the coefficients $A_{lm\alpha}$ and $B_{lm\alpha}$ in Eq. 8.11. A major mathematical difficulty here is that function (8.10) is expressed in a general cylindrical coordinate system and function (8.11), in a local spherical system. However, using the theorem of addition for cylindrical functions, we can express Ψ_{II} through the cylindrical coordinates Z_α, Φ_α and R_α of the sphere α and the local spherical system r, θ, φ:

$$\begin{aligned}\Psi_{II\alpha}(r,\theta,\varphi|k,P,M,N) &= \frac{1}{\sqrt{2\pi c}}\exp\{i(K_P Z_\alpha + M\Phi_\alpha)\}\times \\ &\times \exp\{iK_P r\cos\theta\}(-1)^M\times \\ &\times \sum_{m=-\infty}^{+\infty}\left[C^J_{MN}J_{m-M}\left(\kappa_{|M|,N}R_\alpha\right) + C^Y_{MN}Y_{m-M}\left(\kappa_{|M|,N}R_\alpha\right)\right] \\ &\times J_m\left(\kappa_{|M|,N}r\sin\theta\right)e^{im\varphi}. \end{aligned} \tag{8.13}$$

Now, the coefficients $A_{lm\alpha}$ and $B_{lm\alpha}$ overlap and Hamiltonian integrals can be readily calculated that permits determination of the electron dispersion curves $E(k)$ of nanotube from a secular equation.

Figure 8.1 shows the band structure for the (12, 12) carbon nanotube. The computation results show that the carbon nanotube has a metal-type band structure with the Fermi level located at the intersection of two π-bands at the point $k = (2/3)(\pi/c)$. The density of states near the Fermi level between the first singularities of the valence band and conduction band is constant.

In the center of the Brillouin zone, the upper occupied σ level $\Gamma_v(\sigma)$ is located above the upper occupied π level $\Gamma_v(\pi)$ in all (n, n) carbon nanotubes. In π-electron models, S_{v1} and S_{c1} are the boundary singularities of the valence and conduction bands, respectively, and the minimal gap is $E_{11} = E_{11}(\pi\pi^*) = E(S_{v1}) - E(S_{c1})$. However, as it can be seen in Fig. 8.1, in the center Γ and at the boundary K of the Brillouin zone, the lower $\Gamma_{c1}(\pi)$ and $K_{c1}(\pi)$ states are located below the S_{c1} singularity and form a shoulder under the S_{c1} peak of the density of states. The $S_{v1} - S_{c1}$ gap still corresponds to the direct transition with the minimal energy. The gap $E_{11}(\sigma\pi^*) = E[\Gamma_{c1}(\pi)] - E[\Gamma_v(\sigma)]$ corresponds to the second direct transition.

Figure 8.2 shows the band structure of (13,0) semiconducting carbon nanotube. The boundary singularities of the valence band (S_{v1}) and conduction band (S_{c1}) correspond to the direct ππ* transition at the point Γ, and the minimum gap $E_{11} = E(S_{c1}) - E(S_{v1})$. The dependence of E_{11} on d^{-1} is oscillating (Fig. 8): the $E_{11}(d^{-1})$ function alternates between two curves corresponding to $(n, 0)$ nanotubes for which the remainder upon division of n by 3 is equal to 1 or 2 (n mod 3 = 1 and n mod 3 = 2, respectively). The curve mod 3 = 1 is located above the curve mod 3 = 2. The maximal values $E_{11} = 0.90$ eV and $E_{11} = 0.56$ eV for mod 3 = 1 and mod 3 = 2 correspond to the tubules this

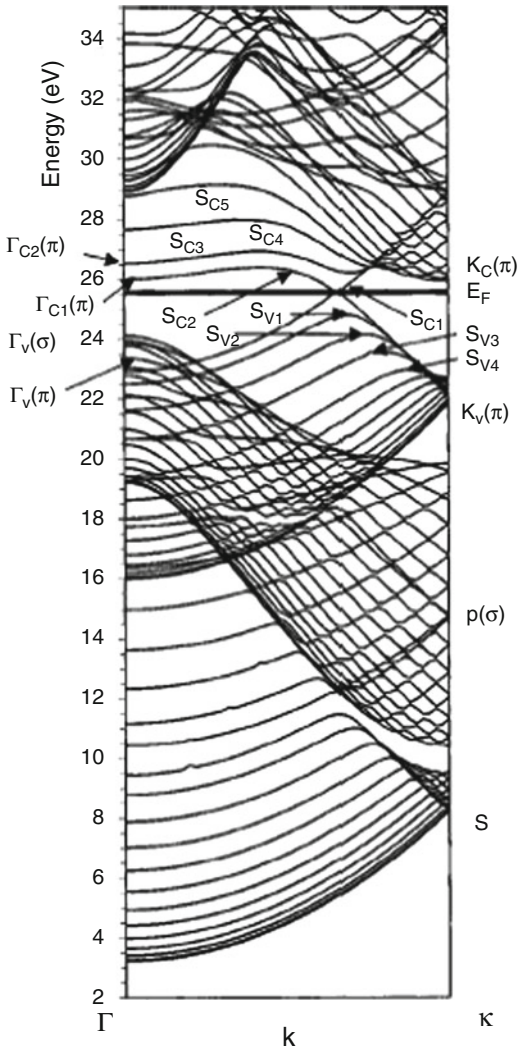

Fig. 8.1 Band structure of the (12, 12) nanotube [6]

$d = 1.25$ ($n = 16$) and 11 Å ($n = 14$), respectively. A further decrease in tube diameter leads to a sharp decrease in the gap E_{11}. For carbon nanotubes with $n \leq 8$ ($d \leq 6.3$ Å), the gap is closed. Figure 8.3 shows that there is not a one-to-one correspondence between E_{11} and d. For example, the E_{11} gap of about 0.3 eV corresponds to four zigzag tubes with $d = 7.8$, 8.6, 20.4, and 40.8 Å. The same is observed for the second direct gap$E_{22} = E(S_{c2}) - E(S_{v2})$. The amplitudes of oscillations of the $E_{22}(d^{-1})$ function are even greater (approximately by a factor of 3) than in the case of $E_{11}(d^{-1})$.

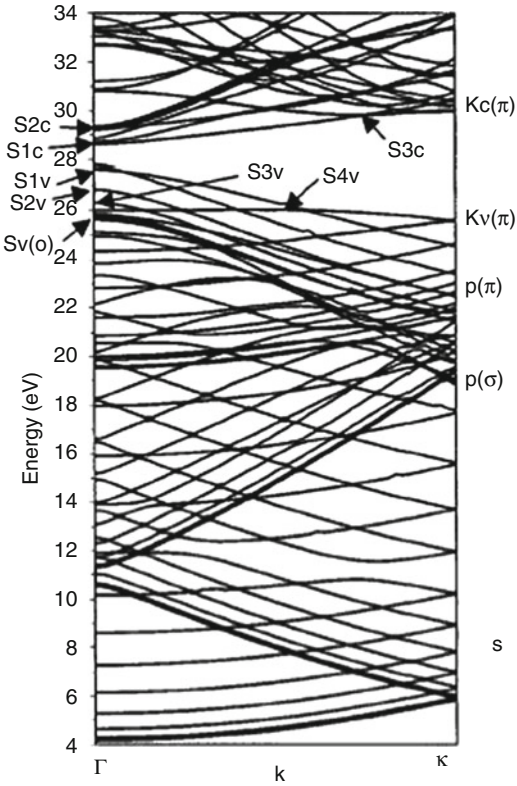

Fig. 8.2 Band structure of the (13,0) nanotube [7]

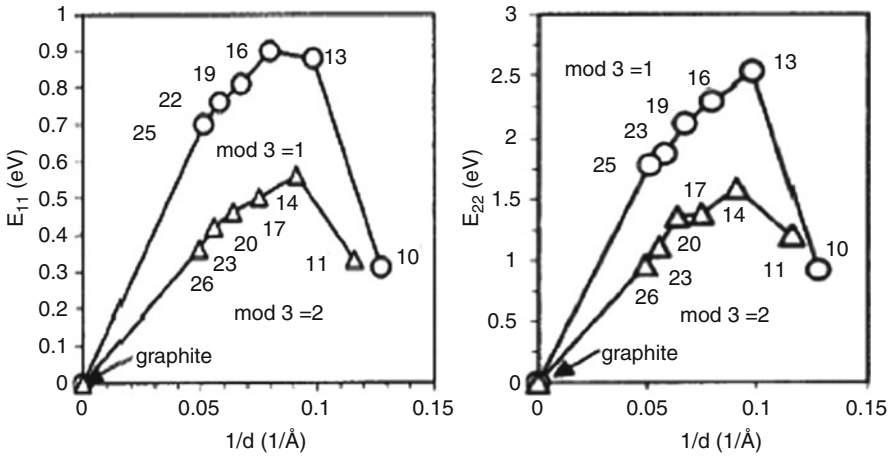

Fig. 8.3 Minimal (E_{11}) and second (E_{22}) optical gaps vs. the diameter of semiconducting (n,0) nanotubes [7]

8.3 Embedded Single-Walled Carbon Nanotubes

Interest has arisen in the design of hybrid electronic devices in which a carbon nanotube is embedded into a common bulk semiconductor. Such devices can be exemplified by electronic elements consisting of a single-walled carbon nanotube embedded into an epitaxially grown semiconductor heterostructure [8]. Let us consider how the interaction with a surrounding crystal can change the band structure of the embedded carbon nanotube.

For an isolated nanotube, there are two vacuum regions Ω_v, on the outside and inside of the nanotube. The nanotube and the vacuum regions are separated by impenetrable (infinite) cylindrical potential barriers. For an embedded nanotube, it is surrounded on the outside with the region of a single-crystal matrix Ω_m. The barrier V_m between the nanotube and the matrix is penetrable (finite), so that tunneling of electrons from the nanotube into the matrix is possible. Let us find the solutions of the Schrödinger equation for the orbitals and electronic energies of the nanotube in the matrix [9, 10]. The matrix is assumed to be a homogeneous medium with a constant potential V_m, which corresponds to the model of a single-walled carbon nanotube in contact with an electron gas. Let us consider the case where the barrier V_m is located noticeably above the Fermi level, so that the matrix has a relatively weak effect on the states of the valence and conduction bands of the nanotube.

In the interspherical region of the nanotube and in the matrix region, the LACWs are the solutions of Schrödinger equation (8.3) with the potential

$$U(R) = \begin{cases} 0, & b \le R \le a \\ \infty, & R<b \\ V_m, & R>b \end{cases}. \tag{8.14}$$

In the matrix region ($U(R) = V_m$), the $\Psi_{|M|N}(R)$ functions must obey the equation:

$$\left[\frac{d^2}{dR^2} + \frac{1}{R}\frac{d}{dR} - \left(V_m - \kappa^2_{|M|,N}\right) - \frac{M^2}{R^2}\right]\Psi_{|M|,N}(R) = 0. \tag{8.15}$$

Equation 8.15 at $V_m > \kappa^2_{MN}$ is a modified Bessel equation. Its solutions when R tends to infinity are modified Bessel functions of the first kind K_M. Thus, at $b \le R \le a$, the LACWs Ψ_{MNP} have the same analytical form as for a separate nanotube, whereas, in the matrix region,

$$\Psi_{PMN}(R) = \frac{C^K_{MN}}{\sqrt{2\pi c}} e^{i(k+k_P)Z} e^{iM\Phi} K_M\left(\kappa^K_{|M|,N} R\right), \tag{8.16}$$

where $\kappa^K_{|M|,N} = \left(V_m - \kappa^2_{|M|,N}\right)^{1/2}$. The analytical expressions for the overlap and Hamiltonian integrals are presented in Makaev and D'yachkov [10].

We studied the effect of the crystalline matrix on the electronic states of metallic (n, n) nanotubes with $4 \le n \le 12$ and semiconducting $(n, 0)$ nanotubes with $10 \le n \le 25$ (n is not a multiple of 3). The delocalization of electrons of a metallic (5, 5)

nanotube into the matrix region leads to a strong disturbance of the band structure. The most important matrix effect is the shift of the σ states located at the point Γ toward higher energies. As a result, the top of the valence σ band Γ_{v1} is shifted into the conduction band and σ electrons start participating in charge transfer. The point of intersection of boundary π bands is shifted toward the edge of the Brillouin zone, and the full width of the valence band is reduced. The metallic character of the band structure of an armchair nanotube persists. In the pristine nanotube, the Fermi level is located at a minimum, and tunneling of electrons into the matrix region leads to the increase in the density of states at the Fermi level.

For semiconducting nanotubes, the minimal gap E_{11} in the center of the Brillouin zone is sensitive to the matrix effect. With a decrease of the barrier V_m, the initial gap E_{11} of nanotube first slightly increases and then sharply decreases and collapses. The described matrix effect is common to nanotubes of all diameters.

Metallization of nanotubes under the action of a matrix as predicted by the model is consistent with the electrical properties of hybrid elements consisting of single-walled nanotubes in semiconducting layers [8]. In all 20 experimentally studied elements, the conductivity at room temperature was independent of the gate voltage; i.e., all nanotubes in crystals turned out to be metallic. (According to statistics, one-third of the tubes, i.e., about seven nanotubes, should be metallic, whereas the rest of them, i.e., about 13 nanotubes, should be semiconducting).

8.4 Double-Walled Nanotubes

Double-walled nanotubes are the simplest case of multiwalled nanotubes. They consist of two concentric cylindrical graphene layers with a strong covalent bond between C atoms in each layer and a weak van der Waals interaction between the layers. From the standpoint of nanoelectronics, double-walled nanotubes are of interest since they are molecular analogues of coaxial cables. The interlayer interaction in a double-walled nanotube has an effect on both the optical and electrical properties of a nanocable.

Let us assume that the cylindrical potential barriers on the outer side of the internal tube and on the inner side of the external tube are penetrable and, hence, tunneling exchange of electrons between the layers of a double-walled tube is possible. In the interspherical region of the nanotube and in the classically impenetrable region between these spheres, the wave functions are the solutions of the Schrödinger equation for the free electron motion, which has its previous form (8.3); however, the potential $U(R)$ in this case has a more complicated form:

$$U(R) = \begin{cases} 0, & b_1 \le R \le a_1, b_2 \le R \le a_2 \\ \infty, & R < b_1, R > a_2 \\ V_f, & a_1 \le R \le b_2 \end{cases}. \tag{8.17}$$

The potential V_f of the interlayer region Ω_f in this model is the only parameter. The potential V_f, the same for all double-walled nanotubes, was selected so that the

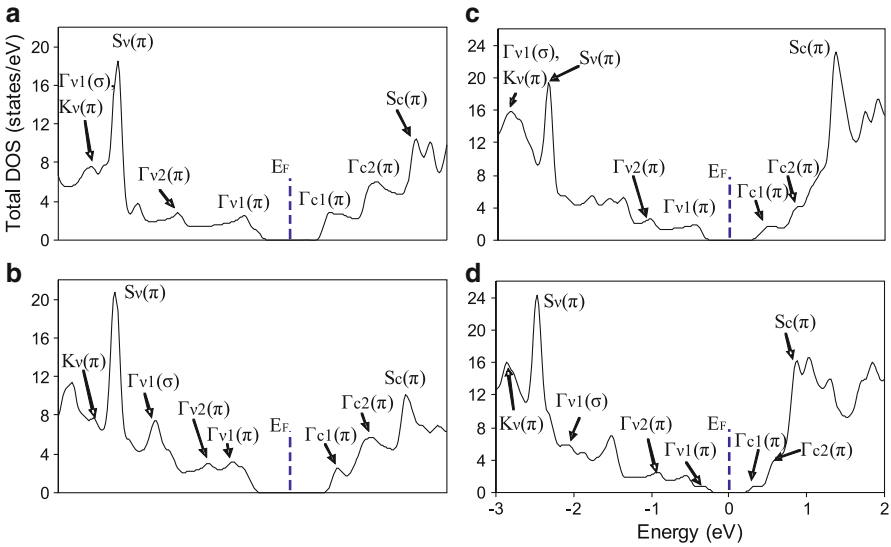

Fig. 8.4 Densities of states near the Fermi level: (**a**) (13,0) single-walled nanotube, (**b**) (13,0) core nanotube nested into the (22,0) nanotube; (**c**) (22,0) single-walled nanotube, and (**d**) the outer (22,0) nanotube with the nested (13,0) tube [11]

level splitting and shifts in the (5,5)@(10,10) nanotube were, on average, 0.5 eV. In the region Ω_f, $U(R) = V_f$, and the $\Psi_{f,|M|,N}(R)$ functions must obey the equation

$$\left[\frac{d^2}{dR^2} + \frac{1}{R}\frac{d}{dR} - \left(V_f - \kappa^2_{|M|,N}\right) - \frac{M^2}{R^2}\right]\Psi_{f,|M|,N}(R) = 0. \tag{8.18}$$

We calculated the electronic levels of a double-walled nanotube located below the potential V_f of the classical forbidden region. Equation 8.18 at $V_f > \kappa^2_{|M|,N}$ is a modified Bessel equation. Its solution is a linear combination of modified Bessel functions of the first K_M and second I_M kinds:

$$\Psi_{f.|M|,N}(R) = C^K_{M,N} K_M\left(\kappa^f_{|M|,N} R\right) + C^I_{M,N} I_M\left(\kappa^f_{|M|,N} R\right), \tag{8.19}$$

where $\kappa^f_{|M|,N} = \left(V_f - \kappa^2_{|M|,N}\right)^{1/2}$. This radial function should vanish at the inner and outer barriers of a double-walled tube and should be continuous and differentiable at the boundaries between the inner and outer tubes and normalized that finally determines the coefficients $C^K{}_{M,N}$ and $C^I{}_{M,N}$ and matrix elements of secular equation for the double-walled nanotubes.

The band structures of double-walled nanotubes can be represented by two structures corresponding to the state of the inner and outer tubes. The full band structure of a double-walled nanotube is a superposition of the band structures of the core and shell tubes [11, 12].

In Fig. 8.4 one can compare the densities of states near the Fermi level of the single-walled (13, 0) and (22, 0) nanotubes with analogous data for the core (13, 0)

and shell (22, 0) tubes in the double-walled system. In the (13, 0)@(22, 0) double-walled nanotube the minimal optical gap (0.83 eV) of the smaller single-walled (13, 0) nanotube is wider than the gap (0.76 eV) of the larger (22, 0) tube. Our calculations show that the minimal optical gap E_{11} of the (13, 0) nanotube increases by 0.19 eV, while that of the (22, 0) nanotube decreases by 0.19 eV after the formation of the double-walled system. The density of states curves near the Fermi level show the analogous decrease in the energy shift of the second gap E_{22} by 0.3 and 0.4 eV for the (13, 0) and (22, 0) nanotubes, respectively. The interlayer interaction leads to the stronger disturbance of the band structure of the inner nanotube as compared to the outer one.

8.5 Single-Walled Chiral Nanotubes

Even for small-diameter chiral nanotubes, the number of atoms in the translational unit cell can be very large. For example, the translational cell of the achiral (10, 10) nanotube comprises 40 atoms, whereas the translational cell of the chiral (10, 9) tube of somewhat smaller diameter comprises 1,084 atoms. The basis set required for the convergence rapidly increases with the increase in the number of atoms in the unit cell, which renders impracticable calculations of chiral tubes. These facts indicate that all rather than only translational symmetry properties of nanotubes should be considered in the development of the theory of their electronic structure [13, 14].

The atomic structure of any single-walled carbon nanotube is determined by two indices (n_1, n_2) and the bond length between carbon atoms. The (n_1, n_2) nanotube has an axis of symmetry C_n, where n is the greatest common factor of the n_1 and n_2 indices. Moreover, the arrangement of atoms of the nanotube is determined by means of screw translations $S(\omega, h)$. Thus, when rotational and screw symmetries are considered, the actual rather than translational unit cell of any nanotube contains only two atoms. If these symmetry properties are taken into account when writing basis wave functions, the electronic structures of any nanotube can be calculated, because the actual rather than translational unit cell of any nanotube contains only two atoms [13, 14].

The cylindrical wave that meets all the symmetry properties is

$$\begin{aligned}
&\Psi_{II,PMN}(Z,\Phi,R|\mathrm{k},L) = \\
&\frac{1}{\sqrt{2\pi h/n}}\exp i\left\{\left[\mathrm{k}+\mathrm{k}_P-(L+nM)\frac{\omega}{h}\right]Z+(L+nM)\Phi\right\} \\
&\times\left[C^{J,L}_{M,N}J_{L+nM}\left(\kappa_{|L+nM|,N}R\right)+C^{Y,L}_{M,N}Y_{L+nM}\left(\kappa_{|L+nM|,N}R\right)\right].
\end{aligned} \tag{8.20}$$

It was used to calculate the band structures of the chiral tubles. For example, the band structure of the (8, 7) nanotube is shown in Fig. 8.5.

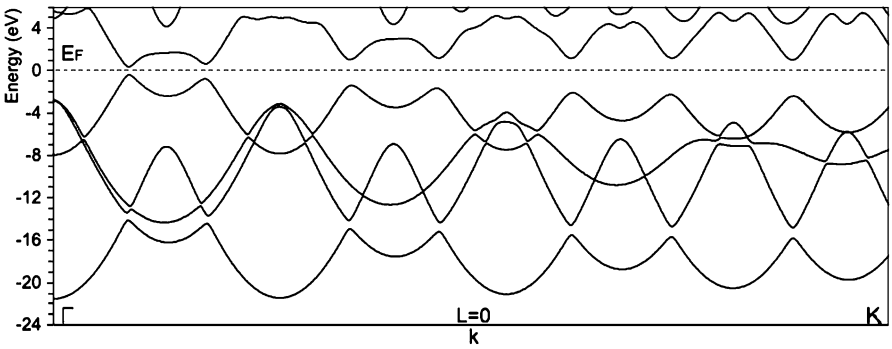

Fig. 8.5 Band structure (8, 7) nanotube [13]

8.6 Single-Walled Nanotubes with Point Defects

Based on the LACW method and Green's function technique, we developed the first-principles numerical method for calculations of the electronic structure of the point impurities in single-walled carbon nanotubes [15]. The host nanotubes electron Green's function is calculated using a linear augmented cylindrical wave theory. The Green's function of the impurities is calculated in terms of matrix Dyson equation. The impurities are described by the single-site perturbed muffin-tin potentials in otherwise perfect nanotubes with the rotational and helical symmetries. Due to the account of these symmetry properties, the method is developed applicable to any tubule including the chiral ones with point defects independent of the number of atoms in translational unit cell of the host systems.

We have determined the local densities of states of the boron and nitrogen impurities in the metallic, semimetallic, and semiconducting tubules. Figure 8.6 shows the typical result of the calculations. It is shown that the boron and nitrogen defects do not destroy the metallic character of electronic structure of the armchair tubules. An increase in the density of states in the Fermi energy region is the most significant effect of boron and nitrogen dopants in the case of metallic and semimetallic nanotubes. In all the semiconducting tubules, in the vicinity of optical gap, there is a drastic difference between the effects of the boron and nitrogen impurities. The boron-related states close the gap of the perfect tubules. In the gap region, the effects of nitrogen atom are restricted with a minor growth of the local density of states just below and above the Fermi energy. Beyond the Fermi-energy region up to the *s* bottom of the valence bands, the effects of impurities are similar in all the tubules. As one goes from carbon to the boron, the local density of states decreases, and the peaks almost disappear, but the nitrogen local density of states is somewhat greater than that of the carbon.

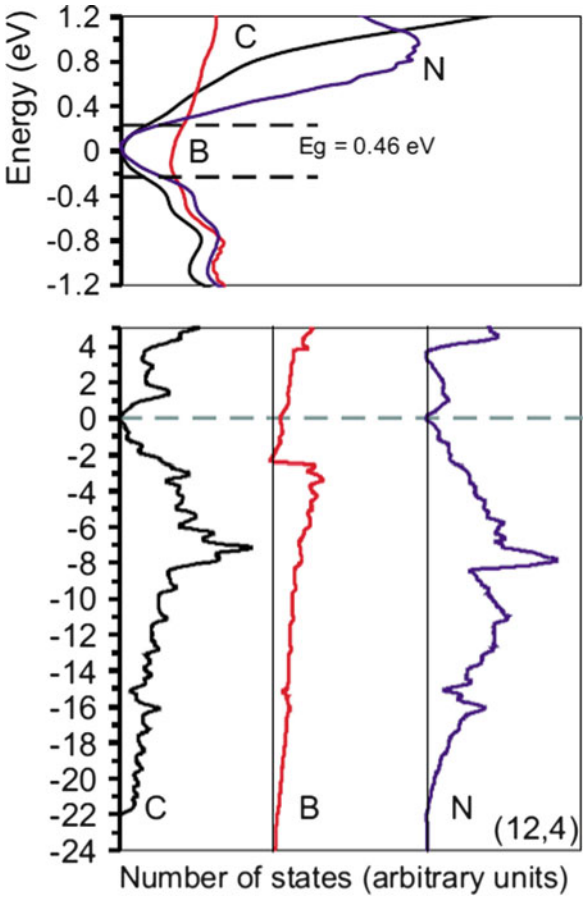

Fig. 8.6 Local densities of states of the ideal and boron and nitrogen doped (12, 4) nanotubes [15]

8.7 Doping of Nanotubes to Control Their Electromagnetic Characteristics

In Nemilentsau et al. [16], the effects of nanotubes doping by either boron or nitrogen on the band structures of the nanotubes were calculated using the LACW method. A metallization of the semiconducting tubules due to the doping was deduced. These results have been used to predict the terahertz and the far-infrared characteristics of small, almost circular bundles of different types of zigzag tubules, as well as those of the composite materials containing such bundles, both before and after chemical modification. It has been shown that the axial surface conductivity of the doped semiconducting nanotubes is significantly higher than that of the undoped ones and can achieve values comparable to the axial surface conductivities of metallic tubules. The electromagnetic responses of such materials for antenna applications can be substantially improved by substitutional doping due to the doping-caused metallization of the semiconducting tubules. We have demonstrated the blue-shift of the antenna resonances frequencies in the

axial-polarizability spectrum of the nitrogen-doped SWNT bundles in comparison to the pristine ones. Increases in the axial polarizability, antenna efficiency, near-field electric-field-intensity enhancement factor, and linear conductivity due to doping have been demonstrated.

Acknowledgments This work was performed in frames of Russian Scientific and Research Program "Scientific and pedagogic personal for innovations in Russia in 2009–2013 years". It was supported by the Russian Basic Research Foundation (grant 11-03-00691) and EU under Project. FP7-247007 CACOMEL.

References

1. D'yachkov PN, Kepp OV, Nikolaev AV (1999) Linearized augmented-cylindrical-wave method in the electronic structure theory of nanowires. Dokl Phys Chem 344(4–6):235
2. D'yachkov PN (2004) Augmented waves for nanomaterials. In: Nalwa HS (ed) Encyclopedia of nanoscience and nanotechnology, vol 1. American Scientific Publishers, Los Angeles, pp 192–212
3. D'yachkov PN, Kirin DV (1999) Extension of the linear augmented-cylindrical-wave method to the electronic structure of nanotubes with an interior hole. Dokl Phys Chem 369(4–6):326
4. D'yachkov PN, Kepp OM (2000) Linear augmented cylindrical wave method for nanotubes: band structure of $[Cu@C_{20}]_{\infty}$. In: Tomanek D, Enbody RJ (eds) Science and application of nanotubes. Kluwer Academic/Plenum Publishers, New York, pp 77–82
5. D'yachkov PN, Kirin DV (2000) Linearized augmented cylindrical wave method and its application to band structure of nanotubes. Ital Phys Soc Conf Proc 74:203
6. D'yachkov PN, Hermann H, Kirin DV (2002) Electronic structure and interband transitions of metallic carbon nanotubes. Appl Phys Lett 81:5228
7. D'yachkov PN, Hermann H (2004) Electronic structure and interband transitions of semiconducting carbon nanotubes. J Appl Phys 95:399
8. Jensen A, Hauptmann JR, Nygerd J, Sadowski J, Lindelof PE (2004) Hybrid devices from single wall carbon nanotubes epitaxially grown into a semiconductor heterostructure. Nano Lett 4:349
9. D'yachkov PN, Makaev DV (2005) Electronic structure of embedded carbon nanotubes. Phys Rev B 71:081101(R)
10. Makaev DV, D'yachkov PN (2005) Linear augmented cylindrical wave method for embedded carbon nanotubes. Dokl Phys Chem 402:109–114
11. D'yachkov PN, Makaev DV (2006) Linear augmented cylindrical wave method for calculating the electronic structure of double-wall carbon nanotubes. Phys Rev B 74:155442
12. Makaev DV, D'yachkov PN (2006) Band structure and optical transitions in semiconducting double-wall carbon nanotubes. JETF Lett 84(5–6):397
13. D'yachkov PN, Makaev DV (2007) Account of helical and rotational symmetries in the linear augmented cylindrical wave method for calculating the electronic structure of nanotubes: towards the *ab initio* determination of band structure of (100, 99) tubule. Phys Rev B 76:057743
14. Makaev DV, D'yachkov PN (2008) Linearized augmented cylindrical wave method for chiral nanotubes. Dokl Phys Chem 419(1):47–53
15. D'yachkov PN, Kutlubaev DZ, Makaev DV (2010) Augmented cylindrical wave Green's function method for electronic structure of nanotubes with substitutional impurities. Phys Rev B 82:035426
16. Nemilentsau AM, Shuba MV, Slepyan GYa, Kuzhir PP, Maksimenko SA, D'yachkov PN, Lakhtakia A (2010) A Substitutional doping of carbon nanotubes to control their electromagnetic characteristics. Phys Rev B 82:235424